



HAL
open science

Exciton interference in hexagonal boron nitride

Lorenzo Sponza, Hakim Amara, François Ducastelle, Annick Loiseau, Claudio Attaccalite

► **To cite this version:**

Lorenzo Sponza, Hakim Amara, François Ducastelle, Annick Loiseau, Claudio Attaccalite. Exciton interference in hexagonal boron nitride. *Physical Review B*, 2018, 97 (7), pp.075121. 10.1103/PhysRevB.97.075121 . hal-01635495

HAL Id: hal-01635495

<https://hal.science/hal-01635495>

Submitted on 15 Nov 2017

HAL is a multi-disciplinary open access archive for the deposit and dissemination of scientific research documents, whether they are published or not. The documents may come from teaching and research institutions in France or abroad, or from public or private research centers.

L'archive ouverte pluridisciplinaire **HAL**, est destinée au dépôt et à la diffusion de documents scientifiques de niveau recherche, publiés ou non, émanant des établissements d'enseignement et de recherche français ou étrangers, des laboratoires publics ou privés.

Exciton interference in hexagonal boron nitride

Lorenzo Sponza, Hakim Amara, François Ducastelle, and Annick Loiseau

LEM UMR 104, ONERA - CNRS, Châtillon, France

Claudio Attaccalite

CINaM UMR 7325, Aix-Marseille University - CNRS, Marseille, France

(Dated: September 22, 2017)

Abstract

In this letter we report a thorough analysis of the exciton dispersion in bulk hexagonal boron nitride. We solve the *ab initio* GW Bethe-Salpeter equation at finite $\mathbf{q} \parallel \Gamma K$, and we compare our results with recent high-accuracy electron energy loss data. Simulations reproduce the measured dispersion and the variation of the peak intensity. We focus on the evolution of the intensity, and we demonstrate that the excitonic peak is formed by the superposition of two groups of transitions that we call KM and MK' from the k-points involved in the transitions. These two groups contribute to the peak intensity with opposite signs, each damping the contributions of the other. The variations in number and amplitude of these transitions determine the changes in intensity of the peak. Our results contribute to the understanding of electronic excitations in this systems along the ΓK direction, which is the relevant direction for spectroscopic measurements. They also unveil the non-trivial relation between valley physics and excitonic dispersion in h -BN, opening the possibility to tune excitonic effects by playing with the interference between transitions. Furthermore, this study introduces analysis tools and a methodology that are completely general. They suggest a way to regroup independent-particle transitions which could permit a deeper understanding of excitonic properties in any system.

Hexagonal boron nitride (h -BN) is a layered crystal whose planes are homostructural to graphene, with B and N atoms occupying alternately the vertices of a honeycomb lattice. It displays peculiar optoelectronic properties, measured notably with luminescence [1–4], X-rays [5, 6] or electron energy loss spectroscopy (EELS) [7, 8]. Though it is established that this material hosts strong excitonic effects, their character (direct or indirect) is still controversial. For instance, theoretical calculations predict h -BN to be an indirect gap insulator [6, 9], but this result contrasts with the experimental finding of strong luminescence in h -BN crystals [1]. Diverse explanations have been proposed to dispell this contradiction [2, 10, 11]. This controversy calls for thorough theoretical investigations and accurate experiments aiming at electronic excitations at finite momentum $\mathbf{q} \parallel \Gamma K$. This indeed is the relevant direction to observe electronic excitations across the indirect gap. Recent very high-quality EELS measurements [7] make a step forward in this direction.

Finite-momentum measurements performed by electron energy loss spectroscopy or X-rays scattering, make possible the observation of excitonic features and of their evolution as functions of frequency ω and exchanged momentum \mathbf{q} . These techniques give access to the loss function

$$L(\mathbf{q}, \omega) = -\text{Im}[1/\epsilon(\mathbf{q}, \omega)] = \text{Im}[\epsilon(\mathbf{q}, \omega)]/|\epsilon(\mathbf{q}, \omega)|^2. \quad (1)$$

Where the dielectric function $\epsilon(\mathbf{q}, \omega)$ is not vanishing, peaks of $L(\mathbf{q}, \omega)$ are related to intra-band transitions. So far, measures have been reproduced, interpreted and even anticipated by *ab initio* simulations based on the Bethe-Salpeter equation (BSE) formalism [12], which includes explicitly the electron-hole interaction (the exciton).

An intriguing behaviour observed in all cases is a sizeable variation of the peak intensity of $L(\mathbf{q}, \omega)$ as a function the exchanged momentum \mathbf{q} , notably the heneancement or attenuation of excitonic peaks along their dispersion [6, 13, 14]. This is actually the case also for the data reported in [7]. The authors give account of a peak dispersing approximately 0.2 eV for $0.1 \text{ \AA}^{-1} \leq \mathbf{q} \leq 1.1 \text{ \AA}^{-1}$ parallel to the ΓK direction of the first Brillouin zone. It detaches neatly from the background, reaches the highest intensity at about 0.7 \AA^{-1} and almost disappears at 1.1 \AA^{-1} . The authors attribute it to an excitonic nature owing to its sharpness. Also, they accompany their experimental data with a tentative analysis based on Kohn-Sham density of states, while calling for the utilization of more advanced methods.

In this letter we solve the *ab initio* BSE in the same energy and momentum conditions as in [7], confirming the excitonic nature of the peak. Also we devise some accurate numerical

tools and carry out a thorough analysis of the peak intensity as a function of the exchanged momentum \mathbf{q} , clarifying the origin of the enhanced intensity at 0.7 \AA^{-1} and its dramatic attenuation at higher momentum. Our study offers a deeper insight into the electronic excitations of h -BN and it unveils a non-trivial valley physics, indicating possible ways to exploit it and to tune the exciton intensity. Furthermore, the framework and the procedures introduced here are of general applicability. We believe that the outcome of our analysis can qualitatively explain similar effects in other materials and that the methods introduced constitute helpful tools to describe and analyse excitonic properties in any system.

Computational details

The simulated h -BN has lattice parameters $a = 2.5 \text{ \AA}$ and $c/a = 2.6$ [15]. The Kohn-Sham system and the GW corrections have been computed with the ABINIT simulation package (a plane-wave code [16]). Norm-conserving Troullier-Martins pseudopotentials have been used for the two atomic species. The DFT energies and wave functions have been obtained within the local density approximation to the exchange-correlation potential, using a plane-wave cutoff energy of 30 Ha and sampling the Brillouin zone with a $8 \times 8 \times 4$ Γ -centred k-point grid. The GW quasiparticle corrections have been obtained on a $6 \times 6 \times 4$ Γ -centred grid, a cutoff energy of 30 Ha defines the matrix dimension and the wave function basis for the exchange part of the self-energy. The correlation part has been computed including 600 bands and the same cutoff energy. To model the dielectric function, the Godby-Needs plasmon-pole approximation [17] has been used, summing over 600 bands and with a matrix dimension of 6.8 Ha. The quasiparticle corrections have been subsequently interpolated on a denser $36 \times 36 \times 4$ k-point grid.

The macroscopic dielectric function $\epsilon(\mathbf{q}, \omega)$ has been calculated at the GW-BSE level in the Tamm-Dancoff approximation using the code EXC [18]. We included six valence bands and three conduction bands; 80 eV and 110 eV respectively are the cutoff energies for the matrix dimension and the wave function basis. The static dielectric matrix entering in the BSE has been computed within the random phase approximation with local fields, including 350 bands and with a cutoff energy of 120 eV and 200 eV for the matrix dimension and the matrix elements respectively. With these parameters, the energy of the first peaks of $\epsilon(\mathbf{q}, \omega)$ are converged within 0.01 eV and their intensity are converged within 5%. All reported

spectra have been convoluted with a Gaussian of $\sigma = 0.05$ eV in order to reduce the noise due to the discrete k-point sampling and to simulate the experimental broadening.

Theoretical analysis tools

EELS and X-ray inelastic scattering give access to the loss function $L(\mathbf{q}, \omega)$ with complementary degrees of accuracy in the \mathbf{q} range [8].

Theory-wise, $L(\mathbf{q}, \omega)$ can be calculated accurately as in (1) from the dielectric function $\epsilon(\mathbf{q}, \omega)$, obtained as a solution of the BSE. This can be cast in the form of an eigenvalue problem whose Hamiltonian is most often written in a basis of independent-particle (IP) transitions $t = (v, \mathbf{k}) \rightarrow (c, \mathbf{k} + \mathbf{q})$ between occupied and empty states of an underlying IP model, e.g. the Kohn-Sham system. Within this framework and accounting only for resonant transitions, the dielectric function reads:

$$\epsilon(\mathbf{q}, \omega) = 1 - \frac{8\pi}{|\mathbf{q}|^2 \Omega} \sum_{\lambda} \frac{I_{\lambda}(\mathbf{q})}{E_{\lambda}(\mathbf{q}) - \omega + i\eta}, \quad (2)$$

where \mathbf{q} lies inside the first Brillouin zone, $E_{\lambda}(\mathbf{q})$ is the energy of the λ th exciton and Ω is the unit cell volume [19]. The spectral intensity

$$I_{\lambda}(\mathbf{q}) = \left| \sum_t \tilde{\rho}_t(\mathbf{q}) A_t^{\lambda}(\mathbf{q}) \right|^2 = \left| \sum_t M_t^{\lambda}(\mathbf{q}) \right|^2 \quad (3)$$

is the modulus squared of a linear combination of IP-transition matrix elements $\tilde{\rho}_t(\mathbf{q}) = \langle v\mathbf{k} | e^{-i\mathbf{q}\cdot\mathbf{r}} | c\mathbf{k} + \mathbf{q} \rangle$ weighted by the exciton wave function components $A_t^{\lambda}(\mathbf{q})$. The exciton λ is called “bright” when $I_{\lambda}(\mathbf{q})$ is sizeably high, and conversely it is called “dark” when $I_{\lambda}(\mathbf{q}) \approx 0$. This can happen if either $\tilde{\rho}_t(\mathbf{q})$ or $A_t^{\lambda}(\mathbf{q})$ or both are negligible for all t , or when IP-transitions interfere destructively leading to a vanishing sum in expression (3). Thus it is sensible to introduce the normalised cumulant weight [13, 20]:

$$\mathcal{J}_{\lambda}(\mathbf{q}, E) = \frac{1}{I_{\lambda}(\mathbf{q})} \left| \sum_{t: E_t \leq E} M_t^{\lambda}(\mathbf{q}) \right|^2 \quad (4)$$

which allows for a visualization of the building-up of the exciton spectral weight as a function of the IP-transition energy E . This function is positively defined and tends asymptotically to 1, but note that it is not necessarily monotonic.

The normalized cumulant weight gives some sort of global information. One can extract further details from $M_t^{\lambda}(\mathbf{q})$, but still it is not an easy quantity to visualise because at given

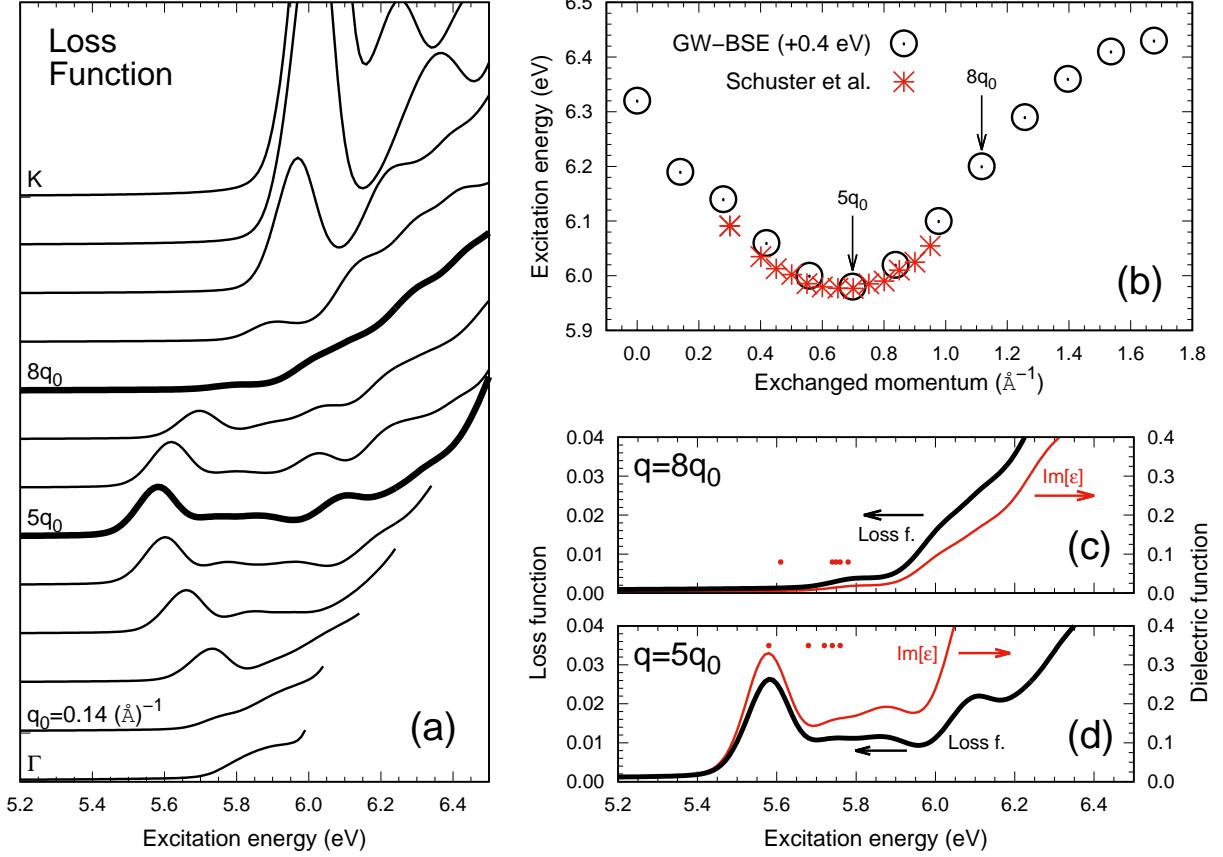


FIG. 1: (a) GW-BSE simulations of the Loss function; thicker lines correspond to $q = 5q_0 = 0.7\text{\AA}^{-1}$ and $q = 8q_0 = 1.1\text{\AA}^{-1}$. (b) Computed dispersion compared to experimental data extracted from [7]. GW-BSE data have been shifted by 0.4 eV. (c,d) Spectra of the loss function (black line) and of $\text{Im}[\epsilon]$ (red line) at $q = 8q_0$ and $q = 5q_0$ respectively. Red bullets mark the position of the first five excitons.

\mathbf{q} and λ it depends on three indexes: $t \equiv (v, \mathbf{k})(c, \mathbf{k} + \mathbf{q})$. Let us define the band-contracted amplitude map:

$$M^\lambda(\mathbf{k}, \mathbf{q}) := \sum_{v,c} M_{(v,\mathbf{k}) \rightarrow (c,\mathbf{k}+\mathbf{q})}^\lambda(\mathbf{q}). \quad (5)$$

This quantity corresponds to the total amplitude of all the transitions from (or to) the \mathbf{k} -point \mathbf{k} (or $\mathbf{k} + \mathbf{q}$). In fact the modulus permits to visualise easily a \mathbf{k} -point cartography of the transitions participating in the exciton formation.

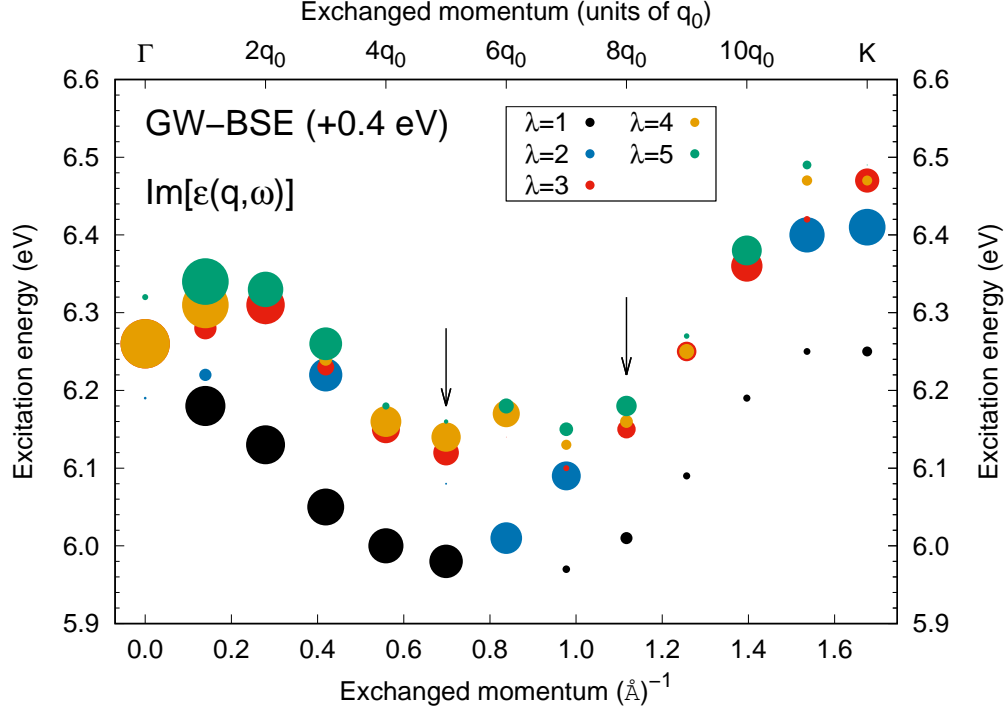


FIG. 2: Simulated dispersion of $E_\lambda(\mathbf{q})$ for $\lambda = 1, 2, 3, 4, 5$. The size of the circles is proportional to $\log I_\lambda(\mathbf{q})$ (see text). GW-BSE data have been shifted up by 0.4 eV. Arrows highlight $\mathbf{q} = 5\mathbf{q}_0$ and $\mathbf{q} = 8\mathbf{q}_0$.

Results

In Figure 1(a) we report the simulated loss function $L(\mathbf{q}, \omega)$ for exchanged momenta $\mathbf{q} \parallel \Gamma K$ at intervals of $\mathbf{q}_0 = K/12 \approx 0.14 \text{ \AA}^{-1}$. The dispersion is reported in Figure 1(b) where it is compared to experimental data extracted from [7]. Beside a blue-shift of about 0.4 eV that comes from a well-known underestimation of the G_0W_0 gap [21] in this material, the calculated spectra and their dispersion are in very good agreement with the measurements. In particular our simulations reproduce the fact that the lowest energy excitation is at $\mathbf{q} = 5\mathbf{q}_0 \approx 0.7 \text{ \AA}^{-1}$ and that approximately at $\mathbf{q} = 8\mathbf{q}_0 \approx 1.1 \text{ \AA}^{-1}$ the peak intensity is strongly suppressed (cfr. Figure 1 in [7]). At higher \mathbf{q} , the loss function increases again with abrupt intensity, reproducing the strong exciton expected at $\mathbf{q} = K$ and already analysed elsewhere in literature [5, 6, 8]. Along the ΓK line, the total dispersion of the loss peak is of about 0.45 eV, which is the energy difference between the peak position at K and at $5\mathbf{q}_0$.

As $|\epsilon(\mathbf{q}, \omega)|$ is not vanishing in the case studied, the peaks of $L(\mathbf{q}, \omega)$ can be directly related

to those of $\text{Im}[\epsilon(\mathbf{q}, \omega)]$, in agreement with equation (1). This is evident from Figures 1(c) and 1(d) where we report the spectra of $L(\mathbf{q}, \omega)$ and $\text{Im}[\epsilon(\mathbf{q}, \omega)]$ at $q = 8q_0$ and $q = 5q_0$ respectively. In order to better understanding the variations of the intensity, we then rely on $\text{Im}[\epsilon(\mathbf{q}, \omega)]$. In Figure 2 we report the calculated dispersion of the excitation energies $E_\lambda(\mathbf{q})$ of the first five lowest-energy excitons as a function of \mathbf{q} ($\lambda = 1, 2, 3, 4, 5$). The size of the circles is proportional to $\log[I_\lambda(\mathbf{q})]$. Their positions are also reported as red bullets in Figures 1(c) and 1(d). From the comparison of Figures ?? and 1(b), it is clear that the dispersion of the first peak of $L(\mathbf{q}, \omega)$ follows closely that of the first bright peak of $\text{Im}[\epsilon(\mathbf{q}, \omega)]$ (6.41 eV and 5.98 eV at K and $\mathbf{q} = 5\mathbf{q}_0$ respectively). Note that these numbers refer to the first intense peak (large circles) which is not always the lowest-energy exciton, i.e. it is not always $\lambda = 1$. In fact, as expected [9, 22, 23], at $\mathbf{q} = \Gamma$ the first two excitons are degenerate and basically dark, whereas all the peak intensity is concentrated on the degenerate excitons with $\lambda = 3$ and 4. As soon as one moves away from Γ , the degeneracy is lifted [23] and the first bright peak coincides with the first exciton. This is valid up to $\mathbf{q} \approx 6\mathbf{q}_0$ (halfway in the ΓK line) where the peak intensity is moved to $\lambda = 2$ as a consequence of a band crossing. The intensity of the excitations is successively reduced at $8\mathbf{q}_0$ and $9\mathbf{q}_0$ where one observes an almost superposition of the $\lambda = 2, 3, 4, 5$ excitons. Finally, as \mathbf{q} approaches K , the exciton $\lambda = 2$ steps-up again concentrating most of the intensity.

In the following we will focus on the excitations at $\mathbf{q} = 5\mathbf{q}_0$ and $\mathbf{q} = 8\mathbf{q}_0$, marked with black arrows in Figures 1(b) and 2.

Analysis of the dielectric function $\epsilon(\mathbf{q}, \omega)$

Exciton analysis at $\mathbf{q} = 5\mathbf{q}_0 \approx 0.7 \text{ \AA}^{-1}$

The excitonic peak at $\mathbf{q} = 5\mathbf{q}_0$ has a binding energy of 0.25 eV, that is the energy difference with respect to the lowest IP-transition with the same \mathbf{q} (including G_0W_0 corrections). In Figure 3 the normalised cumulant spectral function defined in (4) is reported versus the energy E of the IP-transitions. We observe that $\mathcal{J}_{\lambda=1}(\mathbf{q}, E)$ is a monotonic function of E ; it rises steeply up to $E \approx 6.8$ eV from where its derivative decreases mildly. Finally it reaches its asymptotic value of 1 at about $E \approx 12$ eV (not shown). What this tells us is that IP-transitions sum up constructively at all energies, with most important contributions

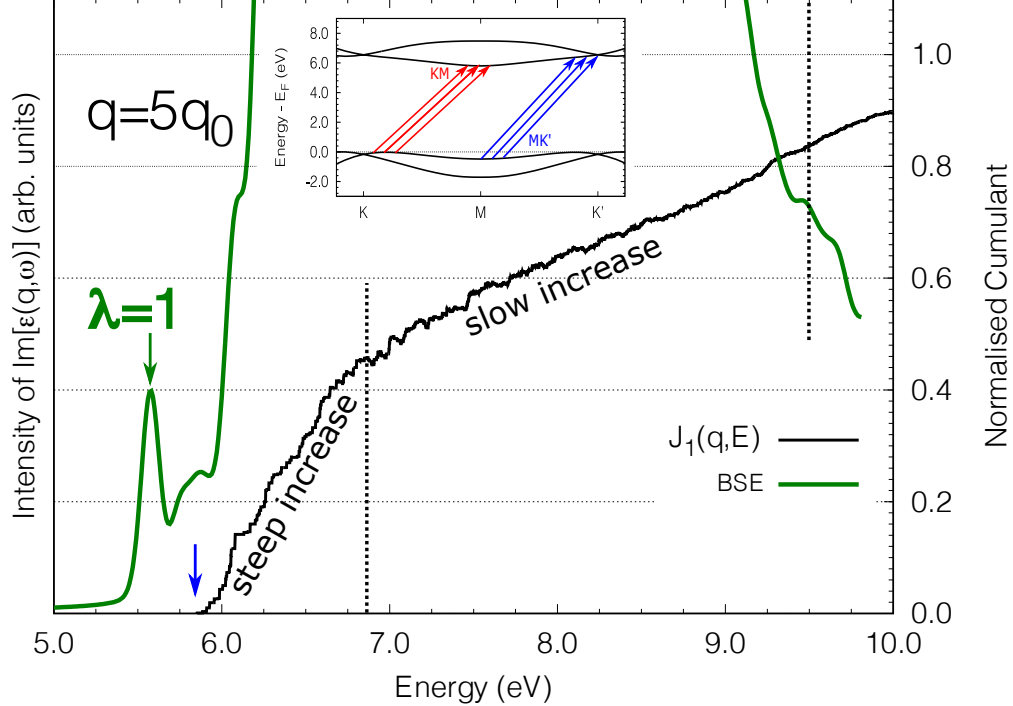


FIG. 3: Cumulant spectral weight (black curve), GW-BSE spectrum (green curve) at $q = 5q_0$. A blue arrow marks the lowest IP-transition. Inset: Sketch of the KM and MK' groups of IP-transitions.

coming from transitions of energy $E < 6.8$ eV. Indeed these few transitions (0.4% of the total) account for almost the 44% of the spectral weight, as $\mathcal{J}_1(5\mathbf{q}_0, 6.8) = 0.44$ attests. Still, to get closer to the full spectral weight, one has to include higher-energy transitions. At $E = 9.5$ eV, 84% of the spectral weight is accounted for by still a relatively small number of transitions (9% of the total).

We can now gain a deeper insight into the way IP-transitions combine in forming the exciton. To do this, let us divide the latter group of transitions ($E \leq 9.5$ eV) in three categories: those for which both real and imaginary parts of $M^\lambda(\mathbf{q})$ are positive, those for which both are negative and transitions where they have opposite sign. The latter group turns out to be composed by transitions with amplitude $M_t^\lambda(\mathbf{q}) \approx 0$, so they do not contribute significantly to the exciton intensity and we can safely neglect them. The other two groups enter the sum of Eq. (3) with different signs. Almost 39% of the considered transitions fall in the first group, with positive amplitude $M_t^\lambda(\mathbf{q})$. They are mostly low-energy transitions. The corresponding cartographies of $|M^{\lambda=1}(\mathbf{k}, \mathbf{q})|$ and $|M^{\lambda=1}(\mathbf{k} + \mathbf{q}, \mathbf{q})|$ for \mathbf{k} -points in the ΓKM -plane are reported in panels (a) and (b) of Figure 4. On the other

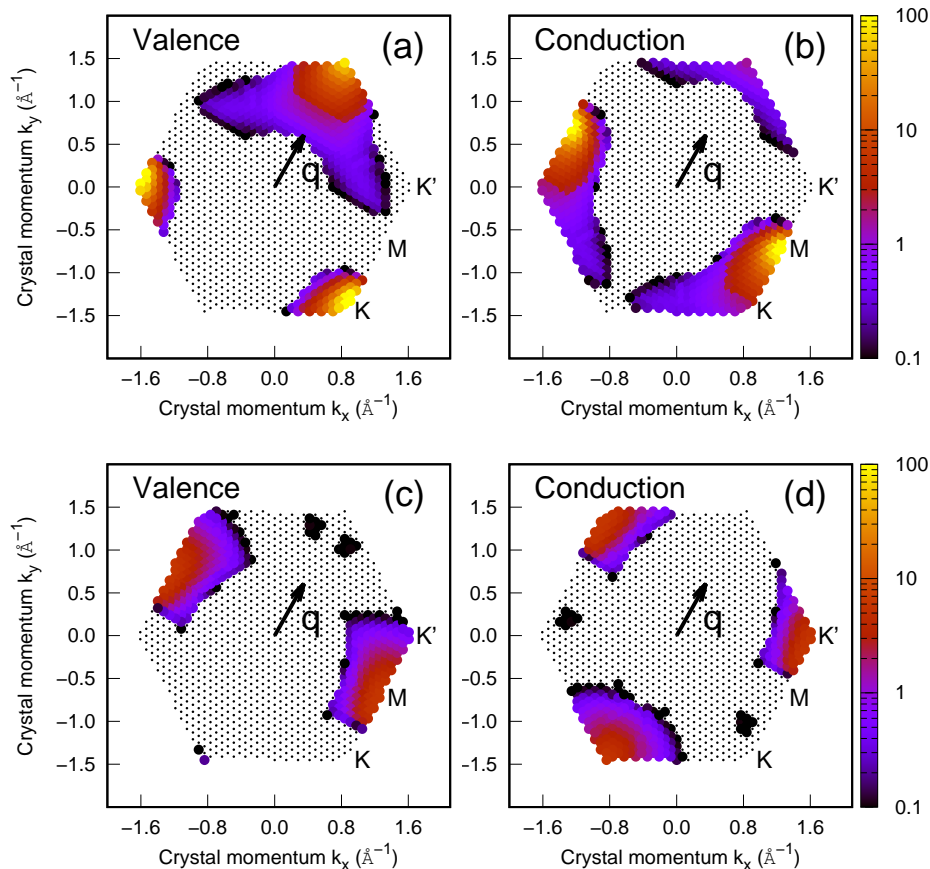


FIG. 4: (Color online) Panels (a) and (b): $|M_1(\mathbf{k}, 5\mathbf{q}_0)|$ and $|M_1(\mathbf{k} + \mathbf{q}, 5\mathbf{q}_0)|$ plotted for \mathbf{k} -points in the ΓKM -plane for transitions of the KM group. Panels (c) and (d): the same for the MK' group.

hand, almost 27% of the considered transitions fall in the negative amplitude group and they have higher energy. Their maps are reported in panels (c) and (d) of Figure 4.

The analysis suggests the following interpretation. Two groups of transitions participate to the formation of the bright exciton ($\lambda = 1$), observed in Ref. [7]. One group (let us call it KM -group) is composed mostly by low-energy transitions going from points close to K to points close to M (and similarly $H \rightarrow L$ in the AHL -plane, not shown). The lowest-energy transitions of this group have also the larger amplitude $M_t^\lambda(\mathbf{q})$, and they sum constructively in the steep part of the cumulant ($E < 6.8$ eV). At higher energy, a second group of IP-transitions (call it MK' -group), from points in the vicinity of M to points in the vicinity of K' (and $L \rightarrow H'$) start entering into the game with a negative amplitude hence eroding partially the contribution of the KM group. This explains why the derivative of

the cumulant reduces starting from 6.8 eV, but is still positive because of the larger number and higher amplitude of the dominating KM group.

Once the origin of the peak has been established, we can now draw the connection with the single-particle band structure. In the inset of Figure 3 we report the GW band structure along the relevant line KMK' , in good agreement with previous calculations [5, 6, 9, 22] and experiments [24]. The KM and the MK' groups of transitions have been sketched with coloured arrows, respectively red and blue. At this \mathbf{q} , the KM group of transitions are basically the indirect transitions between the top valence and the bottom of conduction. The fact that the top valence is close, but does not coincide, with K is consistent with the fact that the lowest excitation is found at $\mathbf{q} < 6\mathbf{q}_0$. The peak is strong here because at this \mathbf{q} the KM transitions take place between van-Hove singularities. The convex curvature of the band structure also explains well why the MK' transitions enter into the game at higher energy and with a lower intensity.

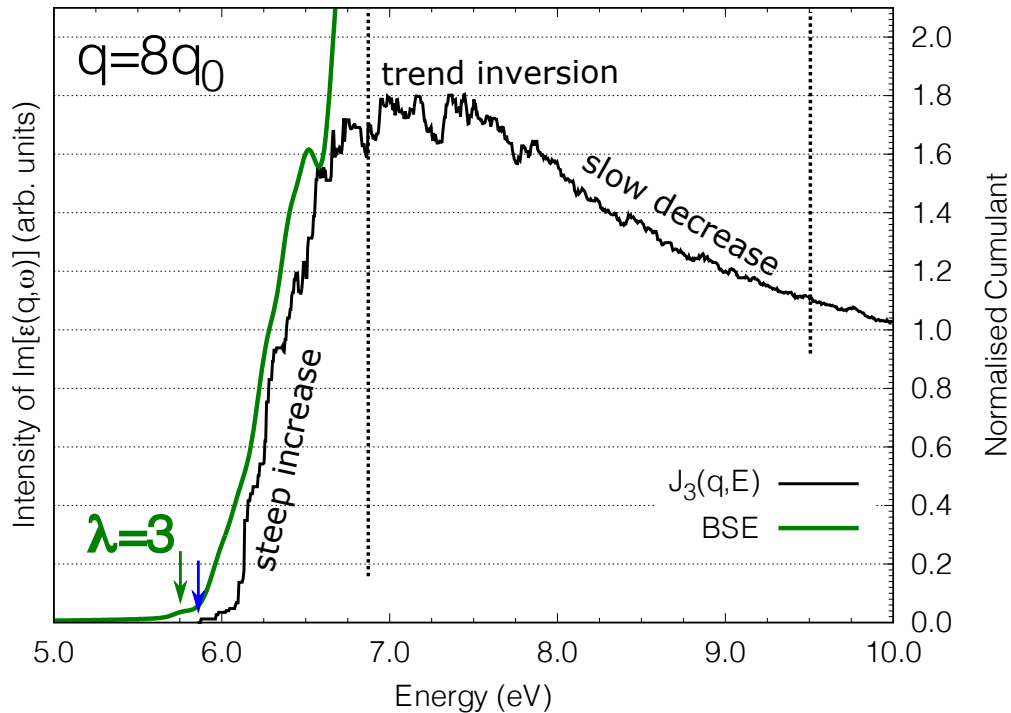


FIG. 5: (Color online) Cumulant spectral weight (black curve), GW-BSE spectrum (green curve). A blue arrow marks the energy of the lowest IP-transition.

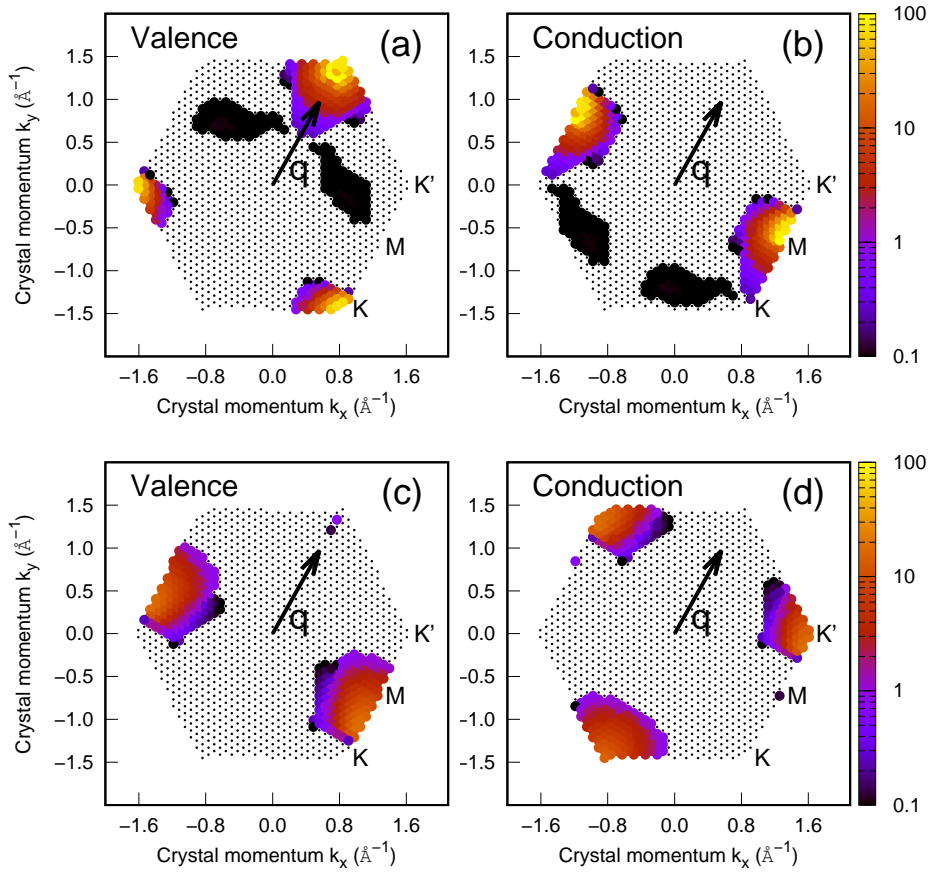


FIG. 6: (Color online) Panels (a) and (b): $|M_3(\mathbf{k}, 8\mathbf{q}_0)|$ and $|M_3(\mathbf{k} + \mathbf{q}, 8\mathbf{q}_0)|$ plotted for \mathbf{k} -points in the ΓKM -plane for transitions of the KM group. Panels (c) and (d): the same for the MK' group.

Exciton analysis at $\mathbf{q} = 8\mathbf{q}_0 \approx 1.1 \text{ \AA}^{-1}$

Let us switch now to $\mathbf{q} = 8\mathbf{q}_0$. At this momentum, the spectral weight is dramatically reduced and it is moved from $\lambda = 1$ to a group of four excitons among which $\lambda = 3$ and $\lambda = 5$ have the highest (although still very weak) intensity. As one can appreciate immediately from the cumulant weight reported in Figure 5, the building-up of the exciton differs significantly from the previous case. In fact, the cumulant function does not grow monotonically, but has instead a concave shape. It increases steeply up to $E \approx 6.8$ eV, it attains its maximum of 1.8 between 7 and 7.8 eV and then decreases to match the asymptotic limit at about 10 eV. This can be rationalized by assuming that most of the IP-transitions entering in $I_\lambda(\mathbf{q})$ sum constructively up to 6.8 eV. But from this energy on, transitions contributing

with opposite sign start having comparable weight. This induces a halt in the increasing trend ($6.8 < E < 7.8$ eV) and eventually they dominate bending down the cumulant back to its asymptotic limit.

Again we focus on the transitions in the energy window $E \leq 9.5$ eV. As before, approximately 9% of the total number of transitions are included. We can again divide the lot into positive and negative amplitudes as before and, not surprisingly indeed, we find that this separation corresponds again to the KM and MK' groups. The band-contracted cartographies are reported in panels (a) and (b) of Figure 6 for the KM group, and (c) and (d) for the MK' group. At variance with the case before, here the number of the transitions is similar (actually slightly larger for MK') and the intensities are closer. The resulting effect is that the two groups of transitions almost cancel each other, leading to a very weak intensity.

It is worth recalling here that this exciton ($\lambda = 3$) is almost degenerate with another non-negligible exciton ($\lambda = 5$). Not surprisingly, carrying out the same analysis on the latter leads to basically the same result, but intriguingly the two groups of transitions have inverted sign: The KM transitions have negative real and imaginary parts of $M_t^\lambda(\mathbf{q})$, while MK' transitions have positive amplitude (not shown).

Conclusions

We solved the *ab initio* GW-Bethe-Salpeter equation at finite \mathbf{q} on bulk h -BN. We report the exciton dispersion of the dielectric function along the direction ΓK of the first Brillouin zone and the corresponding dispersion of the loss function. Its dispersion and intensity agree very closely with recent electron energy loss experiments [7]. In particular, we observe a peak dispersing of about 0.45 eV. It attains its highest intensity at $\mathbf{q} \approx 0.7 \text{ \AA}^{-1}$, corresponding also to the lowest excitation energy. Here it can be associated to the lowest-energy exciton of the dielectric function. At larger momentum $\mathbf{q} \approx 1.1 \text{ \AA}^{-1}$ the peak almost disappears, where it can be associated to two almost degenerate excitons ($\lambda = 3$ and $\lambda = 5$).

With the intent of understanding the origin of this intensity variations, we devised some numerical tools and described them, namely the normalised cumulant weight (4) and the band-contracted amplitude (5). We used these tools to extract different pieces of information about the exciton formation and we successively combined them providing a consistent

interpretation in terms of single-particle transitions.

We showed that two families of transitions participate to the formation of both excitons. One group of transitions (KM) goes from the vicinity of point K to the vicinity of point M , and similarly $H \rightarrow L$ on the AHL -plane. These are low-energy transitions related to the elementary indirect transition of h -BN. The other group of transitions (MK') goes from the vicinity of point M to the vicinity of point K' (and $L \rightarrow H'$ in the AHL -plane). We showed that these transitions contribute with opposite sign and this is at the origin of the damping of the peak at $\mathbf{q} \approx 1.1 \text{ \AA}^{-1}$. Indeed at this momentum, the number of the KM and MK' transitions and their amplitude are comparable, leading to a destructive interference which efficiently damps the peak. Instead at $\mathbf{q} \approx 0.7 \text{ \AA}^{-1}$ the KM transitions are larger in both number and amplitude, thus their contributions dominate leading to a (relatively) strong intensity.

This study adds an important piece of information about the lowest energy excitations in h -BN, especially along the direction ΓK which is the relevant one for spectroscopic measures. The connection between the recently measured excitonic dispersion and the single-particle band structure has been clarified and thoroughly discussed with a particular focus on the variations of intensity. Our investigation has hence allowed us to unveil a non-trivial connection between the exciton dispersion, its intensity and the electronic structure in the vicinity of $K(H)$ and $K'(H')$ points, which may have interesting consequences in the emerging field of valleytronics. This study may inspire specific modifications aiming at controlling the intensity and the dispersion of the lowest-energy excitons in this material by playing with the interference between transitions.

Finally, the methodology presented in this work is of general applicability and could be extended to other systems. In particular, the attenuation of excitons at finite \mathbf{q} has been observed also in other systems and we believe that the explanation given here can be adapted also to all other cases. The criterion adopted to identify constructive and destructive groups of transitions is general, and can be employed in any study of excitons. We believe that this way of classifying the IP-transitions can be very helpful in the analysis and description of excitonic effects in any system.

The authors thank Doctor R. Schuster for the clarifications regarding the experimental data [7]. The research leading to these results has received funding from the European Union H2020 Programme under Grant Agreement No. 696656 GrapheneCore1. We acknowledge

funding from the French National Research Agency through Project No. ANR-14-CE08-0018.

-
- [1] K. Watanabe, T. Taniguchi, and H. Kanda, *Nature Materials* **3**, 404 (2004)
 - [2] G. Cassabois, P. Valvin, and B. Gil, *Nature Photonics* **10**, 262 (2016)
 - [3] P. Jaffrennou, J. Barjon, J.-S. Lauret, B. Attal-Trétout, F. Ducastelle and A. Loiseau, *J. Appl. Phys.* **102**, 116102(2007)
 - [4] L. Schué, B. Berini, A. C. Betz, B. Plaçais, F. Ducastelle, J. Barjon and A. Loiseau, *Nanoscale* **8**, 6986 (2016)
 - [5] S. Galambosi, L. Wirtz, J. A. Soininen, J. Serrano, A. Marini, K. Watanabe, T. Taniguchi, S. Huotari, A. Rubio, and K. Hämäläinen, *Phys. Rev. B* **83**, 081413(R) (2011)
 - [6] G. Fugallo, M. Aramini, J. Koskelo, K. Watanabe, T. Taniguchi, M. Hakala, S. Huotari, M. Gatti, and F. Sottile, *Phys. Rev. B* **92**, 165122 (2015)
 - [7] R. Schuster, C. Habenicht, M. Ahmad, M. Knupfer, and B. Büchner, arXiv:1706.04806v1 (2017)
 - [8] F. Fossard, L. Sponza, L. Schué, C. Attaccalite, F. Ducastelle, J. Barjon, and A. Loiseau, *Phys. Rev. B* **96**, 115304 (2017)
 - [9] B. Arnaud, S. Lebègue, P. Rabiller, and M. Alouani, *Phys. Rev. Lett.* **96**, 026402 (2006) And related comment: L. Wirtz, A. Marini, M. Grüning, C. Attaccalite, G. Kresse, and A. Rubio, *Phys. Rev. Lett.* **100**, 189701 (2008)
 - [10] K. Watanabe and T. Taniguchi, *Phys. Rev. B* **79**, 193104 (2009)
 - [11] L. Museur, E. Feldbach, and A. Kanaev, *Phys. Rev. B* **78**, 155204 (2008)
 - [12] G. Strinati, *La Rivista del Nuovo Cimento* **11**(12), 1-86 (1988)
 - [13] M. Gatti and F. Sottile, *Phys. Rev. B* **88**, 155113 (2013)
 - [14] P.L. Cudazzo, F. Sottile, A. Rubio, and M. Gatti, *J. Phys.: Condens. Matter* **27**, 113204 (2015)
 - [15] V. L. Solozhenko, G. Will, and F. Elf, *Solid State Comm.* **96**, 1 (1995)
 - [16] <http://www.abinit.org/>
 - [17] H. N. Rojas, R. W. Godby, and R. J. Needs *Phys. Rev. Lett.* **74**, 1827 (1995)
 - [18] <http://etsf.polytechnique.fr/exc/>

- [19] G. Onida, L. Reining, and A. Rubio, *Rev. Mod. Phys.* **74**, 601 (2002)
- [20] P. K. Gogoi, L. Sponza, D. Schmidt, T. C. Asmara, C. Diao, J. C. W. Lim, S. M. Poh, S.-I. Kimura P. E. Trevisanutto, V. Olevano, and A. Rusydi, *Phys. Rev. B* **92**, 035119 (2015)
- [21] L. Wirtz, A. Marini, and A. Rubio, *Phys. Rev. Lett.* **96**, 126104 (2006)
- [22] T. Galvani, F. Paleari, H. P. C. Miranda, A. Molina-Sánchez, L. Wirtz, S. Latil, H. Amara, and F. Ducastelle, *Phys. Rev. B* **94**, 125303 (2016)
- [23] J. Koskelo, G. Fugallo, M. Hakala, M. Gatti, F. Sottile and P. Cudazzo, *Phys. Rev. B* **95**, 035125 (2017)
- [24] H. Henck, D. Pierucci, G. Fugallo, J. Avila, G. Cassabois, Y. J. Dappe, M. G. Silly, C. Chen, B. Gil, M. Gatti, F. Sottile, F. Sirotti, M. C. Asensio, and A. Ouerghi, *Phys. Rev. B* **95**, 085410 (2017)